A Simple Geometrically Exact Displacement Based Shell Finite Element

Gustavo C. Gomes[1], Matheus L. Sanchez[1], Paulo M. Pimenta[1], Adnan Ibrahimbegovic[2]

[1]*Polythechnic School at University of São Paulo*
Av. Prof. Almeida Prado, trav. 2 n° 83 Edifício Paula Souza, 05424-970, São Paulo, Brazil
matheus.sanchez@usp.br, gustavocanario@usp.br, ppimenta@usp.br
[2] *Université de Technologie de Compiègne*
Alliance Sorbonne Universités, Laboratoire de Mécanique, Compiègne, France
adnan.ibrahimbegovic@utc.fr

Abstract. This paper presents a modification of the T6-3iKL element based solely on displacements. It is a nonconforming triangular element with 6 nodes and a quadratic displacement field enhanced by a bubble function. Its coefficients are eliminated with three scalar rotation parameters at the mid-side nodes. The element approximates the Kirrchhoff-Love shell model in the large displacement domain with only 21 DoFs . The rotation-continuity between adjacent elements is enforced at mid-side nodes, allowing for multiple branch connections in the mesh. The element allows the adoption of different material constitutive equations. The model is numerically implemented, and the results are compared to varying references in multiple examples, showing the capabilities of the formulation. The original desirable properties of the T6-i3KL element are preserved, which are the lack of penalties or Lagrange multipliers, a simple exact nonlinear kinematics, a relatively small number of DoFs, the possibility of using 3D material models, and is easily connected with multiple branched shells and beams.

Keywords Shell Finite Element Method, Nonlinear, Kirchhoff-Love, Displacement based shell, AceGEN, AceFEM.

1 Introduction

In this work we present an adaptation of the triangular Kirchhoff-Love shell element T6-i3KL developed in [1], creating a new element, hereafter named T6-3iKLED. The present formulation was developed as a collaboration between the authors and firstly presented in [2]. The current work is one in a long arc of publications and developments involving thin shells, composed by, but not limited to, [3], [4], [5], [6], [7], [8] and [1].

The shell element introduced in this paper includes an additional consideration at the mid-side nodes where the shear strain is forced to be zero. This is made with the addition of a bubble-like quartic interpolation of displacements obtained from this consideration. This is achieved without the need for artificial parameters such as penalties. The C1 continuity of the element is ensured at the mid-side nodes using three scalar degrees of freedom (DoF), one for each side of the triangle. The adoption of such enhancement serves not only to minimize the residual shear strain observed in the original element, but also as a step towards analyzing shear stress distribution along the element thickness, due to the quartic interpolation and to all strains described by displacements.

We assume a plane reference configuration for the mid-surface, and the rotation is considered only to obtain the shell's normal director at the mid-side nodes, this being the reference for the additional bubble parameter. In the present work, we have a nonconforming element with 6 nodes, a basic quartic displacement field and a scalar considered at the mid-side nodes, giving in total 21 DoF. The numerical implementation is done using AceGen and AceFEM, fully utilizing the automation of the packages as a mean to obtain physical quantities such as the residual force vector and the stiffness matrix.

In regard to the notation considered throughout the text, italic Latin or Greek lowercase letters (a, b, ..., α, β) denote scalars quantities, bold italic Latin or Greek lowercase letters ($\mathbf{a}, \mathbf{b}, \ldots, \boldsymbol{\alpha}, \boldsymbol{\beta}$) denote vectors, bold italic Latin or Greek capital letters ($\mathbf{A}, \mathbf{B}, \ldots$) denote matrix and second order tensors. Summation convention over repeated indices, with values $\{1, 2, 3\}$ for latin letters and $\{1, 2\}$ for greek letters

2 Shell formulation

2.1 Kinematics

The middle plane is assumed to be in the reference configuration of the shell and is flat, see Fig. 1, with an orthogonal coordinate system $\{\boldsymbol{e}_1^r, \boldsymbol{e}_2^r, \boldsymbol{e}_3^r\}$ where $\boldsymbol{e}_1^r$ and $\boldsymbol{e}_2^r$ are in the middle plane of the shell and $\boldsymbol{e}_3^r$ is normal to the plane. In the current configuration, the orthogonal coordinate system is $\{\boldsymbol{e}_1, \boldsymbol{e}_2, \boldsymbol{e}_3\}$, with the relation $\boldsymbol{e}_i = \boldsymbol{Q}\boldsymbol{e}_i^r$ valid, where $\boldsymbol{Q}$ is the rotation tensor.

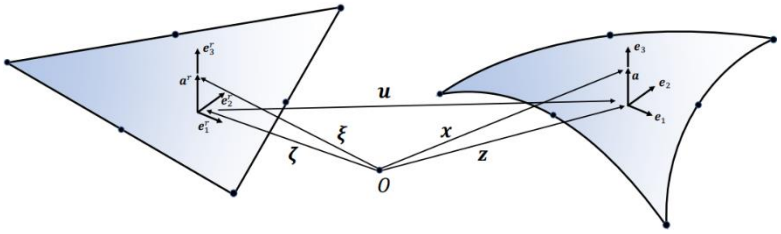

Figure 1 – Shell kinematics

The definition of any point in the reference configuration will then be given by

$$\boldsymbol{\xi} = \boldsymbol{\zeta} + \boldsymbol{a}^r, \boldsymbol{\zeta} = \xi_\alpha \boldsymbol{e}_\alpha^r \in \Omega^r \text{ and } \boldsymbol{a}^r = \zeta \boldsymbol{e}_3^r \in H^r, \tag{1}$$

where $\boldsymbol{\zeta}$ are the coordinates of a material point in the shell middle plane and $\boldsymbol{a}^r$ is the fiber direction of the shell at this point. The thickness h of the shell in the reference configuration is considered through the parameter $\zeta \in \mathrm{H} = [-h^b, h^t]$, where $h = h^b + h^t$.

Similarly to the definition of a material point in the reference configuration, the definition of any point in the current is given by

$$\boldsymbol{x} = \boldsymbol{z} + \boldsymbol{a}, \boldsymbol{z} = \boldsymbol{\zeta} + \boldsymbol{u} \text{ and } \boldsymbol{a} = \boldsymbol{Q}\boldsymbol{a}^r, \tag{2}$$

$\boldsymbol{z}$ represents the current position of a point in the middle surface and $\boldsymbol{a}$ the position along the thickness of the shell, in $\boldsymbol{e}_3$ direction. Here, we remark that $\boldsymbol{Q}$ can be obtained from the shell geometry and displacements.

Adopting the notation $\partial(\cdot)/\partial(\xi_\alpha) = (\cdot)_{,\alpha}$, the deformation gradient can be obtained from:

$$\boldsymbol{F} = \boldsymbol{x}_{,\alpha} \otimes \boldsymbol{e}_\alpha^r + \frac{\partial \boldsymbol{x}}{\partial \zeta} \otimes \boldsymbol{e}_3^r = \boldsymbol{f}_\alpha \otimes \boldsymbol{e}_\alpha^r + \boldsymbol{f}_3 \otimes \boldsymbol{e}_3^r = \left(\boldsymbol{z}_{,\alpha} + \boldsymbol{\kappa}_\alpha \times \boldsymbol{a}\right) \otimes \boldsymbol{e}_\alpha^r + \boldsymbol{Q}\boldsymbol{e}_3^r \otimes \boldsymbol{e}_3^r. \tag{3}$$

Where, as in [3],

$$\boldsymbol{\kappa}_\alpha = axial(\boldsymbol{K}_\alpha) = \boldsymbol{\Gamma}_\beta \boldsymbol{u}_{,\beta\alpha}, \tag{4}$$

$$\boldsymbol{\Gamma}_1 = \left(\boldsymbol{e}_1 \cdot \boldsymbol{z}_{,1}\right)^{-1} \left[\boldsymbol{Skew}(\boldsymbol{e}_1) - \left(\boldsymbol{e}_1 \cdot \boldsymbol{z}_{,2}\right)\left(\boldsymbol{e}_2 \cdot \boldsymbol{z}_{,2}\right)^{-1} (\boldsymbol{e}_1 \otimes \boldsymbol{e}_3)\right], \tag{5}$$

$$\boldsymbol{\Gamma}_2 = \left(\boldsymbol{e}_2 \cdot \boldsymbol{z}_{,2}\right)^{-1} (\boldsymbol{e}_1 \otimes \boldsymbol{e}_3). \tag{6}$$

The curvature vector presented in (4), obtained firstly by [3], is obtained purely with the shell geometry and displacements.

The back-rotated counterparts of the deformation gradient and the strains is defined as

$$\boldsymbol{F}^r = \boldsymbol{Q}^T \boldsymbol{F} = \boldsymbol{I} + \boldsymbol{\gamma}_\alpha^r \otimes \boldsymbol{e}_\alpha^r, \tag{7}$$

with

$$\boldsymbol{\gamma}_\alpha^r = \boldsymbol{\eta}_\alpha^r + \boldsymbol{\kappa}_\alpha^r \times \boldsymbol{a}^r\,; \qquad \boldsymbol{\eta}_\alpha^r = \boldsymbol{Q}^T \boldsymbol{z}_{,\alpha} - \boldsymbol{e}_\alpha^r; \qquad \boldsymbol{\kappa}_\alpha^r = axial\left(\boldsymbol{Q}^T \boldsymbol{Q}_{,\alpha}\right) = \boldsymbol{Q}^T \boldsymbol{\Gamma}_\beta \boldsymbol{u}_{,\beta\boldsymbol{\alpha}} \tag{8}$$

It is important to remark that, due to the Kirchhoff-Love assumption, $\boldsymbol{\gamma}_\alpha^r \cdot \boldsymbol{e}_3^r = \boldsymbol{\eta}_\alpha^r \cdot \boldsymbol{e}_3^r = 0$.

2.2 Displacement field enhancement

The original quadratic displacement field is enhanced using bubble-like displacement functions to generate zero shear strains at the mid-side nodes of the element. The enhanced displacement field interpolation will be given as

$$\boldsymbol{u} = N_1\boldsymbol{u}_1 + N_2\boldsymbol{u}_2 + N_3\boldsymbol{u}_3 + N_4\boldsymbol{u}_4 + N_5\boldsymbol{u}_5 + N_6\boldsymbol{u}_6 + N_{b4}\boldsymbol{u}_{b4} + N_{b5}\boldsymbol{u}_{b5} + N_{b6}\boldsymbol{u}_{b6}, \tag{9}$$

in which $\boldsymbol{u}_1$ up to $\boldsymbol{u}_6$ are the nodal displacements from original nodes and $\boldsymbol{u}_{b4}, \boldsymbol{u}_{b5}$ and $\boldsymbol{u}_{b6}$ are the enhancement displacements. The shape functions from N_1 up to N_6 are the usual quadratic interpolation shape functions in area coordinates and

$$N_{b4} = L_1L_2L_3(1-2L_3), \quad N_{b5} = L_1L_2L_3(1-2L_3), \quad N_{b6} = L_1L_2L_3(1-2L_3) \tag{10}$$

The enhancement functions were selected to ensure that the derivatives relative to the area coordinates do not become zero at the sides, specifically at the mid-side nodes.

Regarding $\boldsymbol{u}_{b4}, \boldsymbol{u}_{b5}$ and $\boldsymbol{u}_{b6}$, these were envisioned as enhancements to the flexural field and are initially defined as

$$\boldsymbol{u}_{b4} = \theta_4 \boldsymbol{e}_{3_4}^{i+1}, \quad \boldsymbol{u}_{b5} = \theta_5 \boldsymbol{e}_{3_5}^{i+1}, \quad \boldsymbol{u}_{b6} = \theta_6 \boldsymbol{e}_{3_6}^{i+1}, \tag{11}$$

where

$$\boldsymbol{e}_{3_4}^{i+1} = \boldsymbol{Q}_{i+1_4} \boldsymbol{e}_{3_4}^r, \quad \boldsymbol{e}_{3_5}^{i+1} = \boldsymbol{Q}_{i+1_5} \boldsymbol{e}_{3_5}^r, \quad \boldsymbol{e}_{3_6}^{i+1} = \boldsymbol{Q}_{i+1_6} \boldsymbol{e}_{3_6}^r, \tag{12}$$

and the scalars θ_4, θ_5 and θ_5 are obtained, with the help of the automated program AceGen, through the use of

$$\begin{aligned} -b_3 \boldsymbol{z}_{,1_4} \cdot \boldsymbol{e}_{3_4}^{i+1} + c_3 \boldsymbol{z}_{,2_4} \cdot \boldsymbol{e}_{3_4}^{i+1} = 0, \\ -b_1 \boldsymbol{z}_{,1_5} \cdot \boldsymbol{e}_{3_5}^{i+1} + c_1 \boldsymbol{z}_{,2_5} \cdot \boldsymbol{e}_{3_5}^{i+1} = 0, \\ -b_2 \boldsymbol{z}_{,1_6} \cdot \boldsymbol{e}_{3_6}^{i+1} + c_2 \boldsymbol{z}_{,2_6} \cdot \boldsymbol{e}_{3_6}^{i+1} = 0. \end{aligned} \tag{13}$$

In the equations above, $b_1, b_2, b_3, c_1, c_2, c_3$, are the usual coefficients obtained from the element nodal coordinates for the area coordinates description and, $\boldsymbol{z}_{,1} = \boldsymbol{e}_1^r + \boldsymbol{u}_{,1}$ and $\boldsymbol{z}_{,2} = \boldsymbol{e}_2^r + \boldsymbol{u}_{,2}$.

2.3 Variational formulation and material equations

The stiffness matrix in this work is obtained through variational formulation with the assistance of AceGen. The usage of this software allows for a plethora of material models readily implemented with automatic differentiation, as long as the material model is given with a strain energy function. In order to assure the convergence of the simulations, we work here with a polyconvex material model suitable for large displacements and rotations.

As the material considered is hyperelastic, a total strain energy function ψ describes the elastic energy stored in the body. Here, we define the functional

$$U = \int_B \left(\psi\big(\boldsymbol{C}(\boldsymbol{u})\big) - \rho_0 \bar{\boldsymbol{b}} \cdot \boldsymbol{u}\right) dV - \int_{\partial B} (\bar{\boldsymbol{t}} \cdot \boldsymbol{u}) dA. \tag{14}$$

One can define the internal total energy for the shell as

$$U^{int} = \int_\Omega \int_{H^r} \psi(\xi_1^r, \xi_2^r) dH d\Omega = \int_\Omega \hat{\psi}(\xi_1^r, \xi_2^r) d\Omega. \tag{15}$$

The strain energy is, obviously, material dependent. The internal stress and material tangent moduli are obtained by

$$\boldsymbol{P} = \frac{\partial \psi}{\partial \boldsymbol{F}} \qquad and \qquad \boldsymbol{D}^r_{\alpha\beta} = \frac{\partial \boldsymbol{\sigma}^r_\alpha}{\partial \boldsymbol{\varepsilon}^r_\alpha} = \frac{\partial^2 \bar{\psi}}{\partial \boldsymbol{\varepsilon}^r_\alpha \partial \boldsymbol{\varepsilon}^r_\beta}. \tag{16}$$

The strain energy function can assume multiple forms in continuum mechanics, with the neo-hookean material being one of the options when dealing with large displacements and deformations. In the current work, the material used is the Ciarlet-Simo Neo-Hookean isotropic material, presented in [9] and defined by the polyconvex strain energy function

$$\psi = \frac{1}{2}\lambda\left(\frac{1}{2}(J^2 - 1) - ln(J)\right) + \frac{1}{2}\mu(I_1 - 3 - 2\,ln(J)), \tag{17}$$

with the invariants, Cauchy-Green stress tensor and Lamé coefficients given as

$$I_1 = tr\,\boldsymbol{C} = \boldsymbol{f}_i \cdot \boldsymbol{f}_i, \quad I_2 = \boldsymbol{tr}(Cof\,\boldsymbol{C}) = \boldsymbol{g}_i \cdot \boldsymbol{g}_i \quad and \quad I_3 = det\,\boldsymbol{C} = J^2 = \left(\boldsymbol{f}_1 \cdot (\boldsymbol{f}_2 \times \boldsymbol{f}_3)\right)^2, \tag{18}$$

$$\boldsymbol{C} = \boldsymbol{F}^T\boldsymbol{F}, \tag{19}$$

$$\lambda = \frac{E\nu}{(1+\nu)(1-2\nu)} \qquad and \qquad \mu = \frac{E}{2(1+\nu)}. \tag{20}$$

2.4 Plane stress

The plane stress condition is a necessity when the shell theory does not consider thickness variation. As such, the present work enforces this condition analytically for the presented materials by adding the term $\boldsymbol{\gamma}^r_{33} = \gamma_{33}\boldsymbol{e}^r_3$ to eq. (7), rewriting it as

$$\boldsymbol{F}^r = \boldsymbol{I} + \boldsymbol{\gamma}^r_\alpha \otimes \boldsymbol{e}^r_\alpha + \boldsymbol{\gamma}^r_{33} \otimes \boldsymbol{e}^r_3. \tag{21}$$

The plane stress is then enforced by $\tau_{33} = \boldsymbol{\tau}^r_3 \cdot \boldsymbol{e}^r_3 = 0$.

With eq. (16), eq. (17) and eq. (21), as seen in [10], one arrives at

$$\tau_{33} = 2(1+\gamma_{33})\frac{\partial \psi}{\partial I_1} + \frac{\partial \psi}{\partial J}\bar{J}, \tag{22}$$

where $\bar{J} = \boldsymbol{e}^r_3 \cdot (f^r_1 \times f^r_2)$**.** After some manipulations, one arrives at

$$\gamma_{33} = \sqrt{\frac{\lambda + 2\mu}{\lambda\bar{J}^2 + 2\mu}} - 1. \tag{23}$$

3 Rotation Field

The rotation field hereby presented is only used to obtain the evolution of the shell's normal director $\boldsymbol{e}_3$. This ensures the C1 continuity of the shell at the mid-side nodes and enforces that the projection of the derivative of the shell's mid-plane position vector $\boldsymbol{e}_3$ is null, guaranteeing zero shear strain at the mid-side nodes.

3.1 Rodrigues rotation vector

The rotation vector can be represented as $\boldsymbol{\theta} = \theta\boldsymbol{e}$, with θ being the rotation around the axis $\boldsymbol{e}$. As presented in [11], the rotation tensor can be a function of the Rodrigues rotation vector as $\boldsymbol{\alpha} = \frac{\boldsymbol{tan}(\theta/2)}{\theta/2}\boldsymbol{\theta}$, restricting the rotation at $-\pi < \theta < +\pi$. As such, the rotation tensor can be defined as

$$\boldsymbol{Q} = \boldsymbol{I} + h(\alpha)\left(\boldsymbol{A} + \frac{1}{2}\boldsymbol{A}^2\right), \quad with \quad h(\alpha) = \frac{4}{4+\alpha^2}, \tag{24}$$

$\alpha = \|\boldsymbol{\alpha}\|$ and $\boldsymbol{A} = \boldsymbol{Skew}(\boldsymbol{\alpha})$**.**

3.2 Incremental description of rotation

The incremental rotational variables are presented as

$$\boldsymbol{Q}_{\Delta} = \boldsymbol{I} + h(\alpha_{\Delta})\left(\boldsymbol{A}_{\Delta} + \frac{1}{2}\boldsymbol{A}_{\Delta}^{2}\right), \quad with \quad h(\alpha_{\Delta}) = \frac{4}{4+\alpha_{\Delta}^{2}}, \tag{25}$$

where $\alpha_{\Delta} = \|\boldsymbol{\alpha}_{\Delta}\|$ and $\boldsymbol{A}_{\Delta} = Skew(\boldsymbol{\alpha}_{\Delta})$.

The update of the rotation tensor is done incrementally by

$$\boldsymbol{\alpha}_{i+1} = \frac{4}{4-\boldsymbol{\alpha}_i \cdot \boldsymbol{\alpha}_{\Delta}}\left(\boldsymbol{\alpha}_i + \boldsymbol{\alpha}_{\Delta} - \frac{1}{2}\boldsymbol{\alpha}_i \times \boldsymbol{\alpha}_{\Delta}\right), \tag{26}$$

where $\boldsymbol{\alpha}_{i+1}$ is the next step of $\boldsymbol{\alpha}_{\mathrm{i}}$. We also update the rotation tensor following the relations

$$\boldsymbol{Q}_{i+1} = \boldsymbol{Q}_{\Delta}\boldsymbol{Q}_i, \ with \ \ \boldsymbol{Q}_{i+1} = \hat{Q}(\boldsymbol{\alpha}_{i+1}), \quad \boldsymbol{Q}_{\Delta} = \hat{Q}(\boldsymbol{\alpha}_{\Delta}) \quad and \quad \boldsymbol{Q}_i = \hat{Q}(\boldsymbol{\alpha}_i). \tag{27}$$

As $\boldsymbol{Q}$ applies to the shell director, one may also define

$$\boldsymbol{e}_3^{i+1} = \boldsymbol{Q}_{\Delta}\boldsymbol{e}_3^{i}. \tag{28}$$

Here we bring the description of the rotation vector in relation to a scalar parameter φ_{Δ}, first presented in [12] in relation to vector $\boldsymbol{e}_3$ and, here, described in relation to $\boldsymbol{e}_1$ to obtain the rotation vector in agreement with [1]. This is done as $\boldsymbol{e}_1$ can be calculated only by displacement. As so, we have

$$\boldsymbol{\alpha}_{\Delta} = \frac{\boldsymbol{e}_1^{i} \times \boldsymbol{e}_1^{i+1}}{\|\boldsymbol{e}_1^{m}\|^2} + \varphi_{\Delta}\frac{\boldsymbol{e}_1^{m}}{\|\boldsymbol{e}_1^{m}\|}, \quad with \quad \boldsymbol{e}_1^{m} = \frac{1}{2}\left(\boldsymbol{e}_1^{i+1} + \boldsymbol{e}_1^{i}\right). \tag{29}$$

At every step, the increment parameters are reset as $\boldsymbol{\alpha}_{\Delta} = \boldsymbol{0}$, $\varphi_{\Delta} = 0$.

4 The Finite Element

The element used is an extrapolation of the T6-3iKL seen in [1], a six-noded displacement-based triangular element (see Fig. 2). The discretization of the element coordinates and displacement field is done with area coordinates and quartic interpolation and, an additional scalar rotation parameter (φ_{Δ}). This model renders a quite efficient element, with a reduced number of DoF when compared with usual models that consider the rotation using three-dimensional vectors as DoF. The enhancement used in order to zero the shear strain is done at element level, not necessitating additional DoF at the global level.

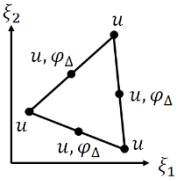

Figure 2 – T6-i3KL

This recent description of the rotation, proposed in [1] is a quite interesting adoption, reducing the number of DoF involved in the analysis while not reducing the quality of results.

The element uses 3 integration points at the mid-side nodes of the shell plane and, when integrating along the thickness, each layer has 3 integration points, using Gauss rule.

5 Results

5.1 Cantilever Beam

The cantilever beam was an example proposed in [13], revisited in [14], [10] and [1] to analyze the behavior

of the element when used under conditions of high rotations and displacement in and out of plane. As for the geometry and the mesh, shown in Fig. 3, a cross section of $b \times h = 0.1 \times 0.1$ is used, with length $L = 1.0$. One end of the beam is clamped, while the other is subjected to a concentrated force $P = 1000$. The beam Neo-Hookean material model has an Young's modulus $E = 10^7$ and poisson's ratio $v = 0.3$.

The comparison values are the results of displacement of the midpoint of the free end of the beam, which are compared with that obtained in the work of [14], where the maximum deflection are $u_{in-plane} = 0.8425$ and $u_{out-of-plane} = 0.8406$. The results indicate that due to the enhancement, as expected, a higher displacement is observed.

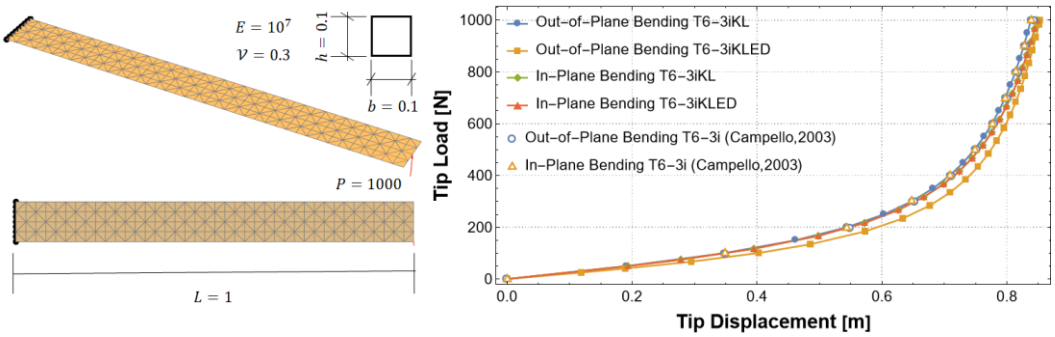

Figure 3 – In and out of plane cantilever beam

5.2 Raasch Challenge

The Raasch challenge serves as a benchmark for shell finite elements. In this challenge, the coupling of shear, twist, extension, and bending modes of deformation is crucial, making it a valuable test for shell elements. The problem involves a curved strip hook with defined radii and geometry. The first radius is $R1 = 14\ in$, the second radius is $R2 = 46\ in$, width of the hook is $w = 20\ in$, and the thickness is $t = 2\ in$. The left end of the strip is clamped, and the free end is subject to a distributed in-plane shear. The material properties of the shell are $E = 3300\ psi$ and $\nu = 0.35$. The geometry, load conditions and material properties are presented in Figure 4.

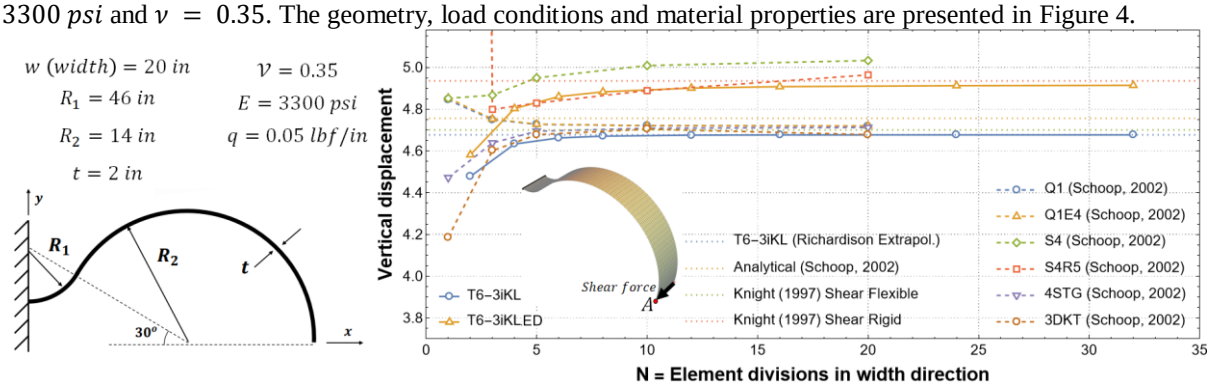

Figure 4 – Raasch challenge

Regarding the results, multiple references are presented in Figure 4, with the main results are associated with T6-3iKL and T6-3IKLED. The first element is comparable with the shear rigid analytical result from [15] and limited by Richardson extrapolation (see [16]) related to mesh refinement. The enhanced element, focus of the current work, is close to the analytical solution of [17], in which no shear deformation is considered, in alignment with the enhancement objective.

6 Conclusions

As seen in the current work, the context of a thin shell with Kirchhoff-Love theory with the enhancement,

create an extremely simple finite element. The results from the numerical implementation indicate that, although simple, the enhancement worked extremely well, indicating a considerable reduction of the shear strain residual observed in the T6-3iKL while maintaining its qualities, these being the lack of penalties or Lagrange multipliers, a simple exact nonlinear kinematics, a relatively small number of DoFs, the possibility of using 3D material models, and easy connectability with multiple branched shells and beams. For the next step, the authors are already working on a multilayer associated theory.

Acknowledgements. Gustavo C. Gomes acknowledges the financial support by CNPq and all the authors thankfully acknowledges FAPESP (contract/grant number: 2020/13362-1).

Authorship statement. The authors hereby confirm that they are the sole liable persons responsible for the authorship of this work, and that all material that has been herein included as part of the present paper is either the property (and authorship) of the authors, or has the permission of the owners to be included here.

References

[1] SANCHEZ, M. L., PIMENTA, P. M., IBRAHIMBEGOVIC, A., "A simple geometrically exact finite element for thin shells — Part 1: statics," *Computational Mechanics*, Vol. 72, pp. 1119–1139, 2023.

[2] SANCHEZ, M. L., "A new fully nonlinear finite element for thin shells", São Paulo: Tese (Doutorado) - Polytechnic School of University of São Paulo, 2024.

[3] PIMENTA, P.M., NETO, E., CAMPELLO, E. M. B., "A Fully Nonlinear Thin Shell Model of Kirchhoff-Love type," *New Trends in Thin Structures: Formulation, Optimization and Coupled Problems*, pp. 29-58, 2010.

[4] VIEBAHN, N., PIMENTA, P. M., SCHRÖDER, J., "A simple triangular finite element for nonlinear thin shells: statics, dynamics and anisotropy," *Computational Mechanics*, vol. 59, no. 2, pp. 281-297, 2017.

[5] SANCHEZ, M. L., PIMENTA, P. M., SILVA, C. C., "A simple fully nonlinear kirchhoff-love shell finite element," *Latin American Journal of Solids and Structures*, vol. 17, no. 8.

[6] SILVA, C.C., MAASSEN, S. F., PIMENTA, P. M., SCHRÖDER, J., " On the simultaneous use of simple geometrically exact shear-rigid rod and shell finite elements," *Computational Mechanics*, vol. 67, no. 3, pp. 867-881, 2021.

[7] SOUSA, C.A.G., SANCHEZ, M. L., GOMES, G. C., PIMENTA, P. M., "Nonlinear Kirchhoff-Love Shell Finite Element: Two Simple Triangular Shell Element," in *Proceedings of the XLIII Ibero-Latin-American Congress on Computational Methods*, Foz do Iguaçu, Brazil, 2022.

[8] GOMES, G. C., PIMENTA, P. M., IBRAHIMBEGOVIC, A., "A simple triangular multilayer Kirchhoff-Love shell element," in *Proceedings of the XLIV Ibero-Latin American Congress on Computational Methods in Engineering*, Porto, Portugal, 2023.

[9] SIMO, J., HUGHES, T., Plasticity and viscoplasticity: Numerical analisys and computational aspects, Berlim: Springer-Verlag, 1991.

[10] CAMPELLO, E. M. B., PIMENTA, P. M., WRIGGERS, P., "A triangular finite shell element based on a fully nonlinear shell formulation," *Computational Mechanics*, vol. 31, pp. 505-518, 2003.

[11] CAMPELLO, E. M. B., PIMENTA, P. M., WRIGGERS, P., "A triangular finite shell element based on a fully nonlinear shell formulation," *Computational Mechanics*, vol. 31, pp. 505-518, 2003.

[12] SILVA, C., MAASSEN, S., PIMENTA, P.M., SCHRÖDER, J., "A simple finite element for the geometrically exact analysis of bernoulli–euler rods," *Computational Mechanics*, pp. 1-19, 2019.

[13] SIMO, J. C., FOX, D. D., RIFAI, M. S., "On a stress resultant geometrically exact shell model. Part III: computational aspects of the nonlinear theory," *Comp. Meth. Appl. Mech. Engrg.*, pp. 21-70, 1990.

[14] WRIGGERS, P., GRUTTMANN, F., "Thin shells with finite rotations formulated in Biot stresses: theory and finite element formultation," *Int. J. Numer. Meth. Engrg.*, pp. 2049-2071, 1993.

[15] KNIGHT JR, N.F., "Raasch challenge for shell elements," *AIAA journal*, vol. 35, no. 2, pp. 375-381, 1997.

[16] KRYSL, P., Finite element modeling with abaqus and python for thermal and stress analysis, San Diego: Petr Krysl, 2017.

[17] SCHOOP, H., HORNIG, J., WENZEL, T., "Remarks on Raasch's hook," *Technische Mechanik-European Journal of Engineering Mechanics*, vol. 22, no. 4, pp. 259-270, 2002.